Available online at www.sciencedirect.com
ScienceDirect
Bioelectrochemistry 69 (2006) 1 – 9
Bioelectrochemistry
www.elsevier.com/locate/bioelechem

DNA-based electrochemical biosensors for monitoring of *bis*-indoles as potential antitumoral agents, chemistry, X-ray crystallography

Dorota Maciejewska [a,*], Iwona Szpakowska [c,d], Irena Wolska [b,*], Maria Niemyjska [a], Marco Mascini [d], Magdalena Maj-Żurawska [c,*]

[a] *Department of Organic Chemistry, Faculty of Pharmacy, Medical University of Warsaw, Banacha 1, 02 097 Warsaw, Poland*
[b] *Department of Crystallography, Faculty of Chemistry, Adam Mickiewicz University, Grunwaldzka 6, 60-780 Poznań, Poland*
[c] *Faculty of Chemistry, University of Warsaw, Pasteura 1, 02-093 Warsaw, Poland*
[d] *Department of Chemistry, University of Florence, Via della Lastruccia 3, 50019 Sesto Fiorentino (FI), Italy*

Received 19 April 2005; received in revised form 25 August 2005; accepted 7 September 2005
Available online 22 November 2005

Abstract

Facile and practical electrochemical DNA bioassay, X-ray diffraction analysis, synthesis and ^{1}H and ^{13}C NMR data of the 5,5′-disubstituted-3,3′-methanediyl-*bis*-indoles are reported. On the basis of electrochemical measurements we have hypothesized that the analyzed *bis*-indoles have an effect on human tumor cells due to DNA binding at adenine-thymidine deoxynucleotides rich region in a concentration/substituent dependent manner. Interesting N–H···π and hydrogen-bonding intermolecular interactions were observed which may differentiate their biological features. The 5,5′-dimethoxy-3,3′-methanediyl-*bis*-indole (**2**) was found to reduce considerably the growth of cancer cell lines HOP-92 (lung), A498 (renal) and MDA-MB-231/1TCC (breast). The results indicate that title compounds could be interesting as potential antitumoral chemotherapeutics.

Keywords: Electrochemical DNA biosensors; 5,5′-Disubstituted-3,3′-methanediyl-*bis*-indoles; X-ray crystallography; Cytotoxicity

1. Introduction

Nowadays DNA biosensors are widely used in different research fields in food, environmental and clinical analysis. Some recent applications have been reported to Genetically Modified Organism detection (GMO) in food [1] by the use of developed Quartz Crystal Microbalance sensors. Many molecules show a high affinity to nucleic acids and they can interact with DNA immobilized on the electrode surface that gives a lot of possibilities for practical use [2]. Nucleic acids offer the analytical chemist a powerful tool in the recognition and monitoring of many important compounds. DNA biosensor technologies are currently under intensive investigation owing to their great promise for rapid and low-cost detection of specific DNA sequences in human, viral and bacterial nucleic acids [3].

In this work, we propose the electrochemical DNA-based biosensor as a screening device for the rapid detection of chemical compounds that are potential antitumor agents interacting with double helix of the nucleic acid. This kind of experiment can be very useful during designing and synthesis new chemical compounds that are potential medicaments especially in the case of cancer to describe their affinity–what means efficacy of treatment–to DNA.

It seems that certain compounds found in the diet could be a potential source of new classes of chemotherapeutic and chemopreventive agents. Human foodstuffs contain indoles that inhibit the carcinogenic process or are tumor promoters in animal model [4–6]. Indole-3-carbinol (**1a**), a major indole metabolite from cruciferous vegetables, and its natural condensation product 3,3′-diindolylmethane (**1**) (Fig. 1), have been found to inhibit the development of tumors in breast, uterus and liver [7–9].

* Corresponding authors. Dorota Maciejewska is to be contacted at Department of Organic Chemistry, Faculty of Pharmacy, Medical University of Warsaw, Banacha 1, 02 097 Warsaw, Poland. Tel./fax: +48 225720643. Irena Wolska, Department of Crystallography, Faculty of Chemistry, Adam Mickiewicz University, Grunwaldzka 6, 60-780 Poznań, Poland. Magdalena Maj-Żurawska, Faculty of Chemistry, University of Warsaw, Pasteura 1, 02-093 Warsaw, Poland.
E-mail addresses: domac@farm.amwaw.edu.pl (D. Maciejewska) iwolska@amu.edu.pl (I. Wolska), mmajzur@chem.uw.edu.pl (M. Maj-Żurawska).

1567-5394/$ - see front matter © 2005 Elsevier B.V. All rights reserved.
doi:10.1016/j.bioelechem.2005.09.003

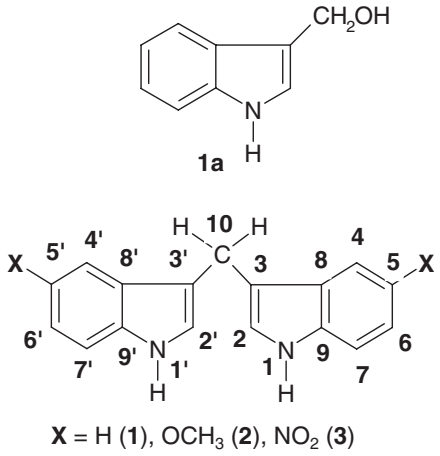

Fig. 1. Chemical formulas and atom numbering; **1a**—indole-3-carbinol; **1**—3,3′-diindolylmethane; **2** and **3**—derivatives of **1**.

However, both compounds may exhibit adverse tumor promoting activity in other organs [5,10]. The studies [9,11,12] concerning their activity against breast cancer showed that compound **1** induced apoptosis by changing the Bax/Bcl-2 ratio and can induce a G1 cell-cycle arrest of human MCF-7 breast cancer cells by stimulation of p21 gene expression as a target. Analysis of protein–DNA complexes isolated from indole **1a**-treated cancer cells has demonstrated that its condensation product **1** accumulates in the nucleus and stimulates the p21 transcription through Sp1 transcription factor, which regulates expression by binding to specific GC-rich DNA fragments. On the other hand, *bis*-indoles could interact with DNA by classic minor groove binding via interactions within the AT-rich region [13]. Small variations of the chemical structure of **1** may modify the transmission of antiproliferative signals. On the basis of this knowledge, we decided to investigate the compounds structurally related to the 3,3′-diindolylmethane (**1**), but bearing two methoxy electron donating groups (compound **2**) [14] or two nitro electron withdrawing groups (compound **3**) on C5/C5′ atoms of the indole rings (Fig. 1). Several researches have reported [15–17] control of binding of small molecules to DNA through the measurements of the electrochemical signal of guanine. In this paper we report the application of the electrochemical system within novel protocol to the analysis of DNA damage due to *bis*-indoles interaction, as a peak height ratio of guanine and adenine signals from double-stranded *calf thymus* DNA (dsDNA), in comparison with **1** selected as a reference compound. Moreover, we have gained further information for compound **2** about cytotoxity against 60 cancer cell lines from the Division of Cancer Treatment and Diagnosis National Cancer Institute (Bethesda, USA).

An attempt to rationalize the relationships between structural features of **1**, **2**, **3** and their interaction with DNA was made on the basis of X-ray diffraction measurements.

The present paper describes guanine and adenine signals analyses employing electrochemical DNA biosensors, chemistry of tested compounds (with so far unpublished ^{1}H and ^{13}C NMR data), cytotoxicity, and single crystal X-ray diffraction studies.

2. Experimental

2.1. Synthesis of 1 and 3

The synthesis, X-ray structure, and physical properties of the 5,5′-dimethoxy-3,3′-methanediyl-*bis*-indole (**2**) were previously reported [14]. The remaining compounds **1** and **3** were newly synthesized from the corresponding indoles and formaldehyde in a one-step process according to the reported procedure [18,19] with slight modifications. The reaction and purification processes were performed out of the light. It was not necessary to keep the reaction vessel under nitrogen to receive a sufficient yield (33–47%). The reactants were solved in water/ethanol solution, vol. 114:30 mL with 0.04 mL conc. sulfuric acid. Melting points were determined with a Digital Melting Point Apparatus 9001 and are uncorrected. The products were purified by repeated crystallization from ethanol. Reagents were obtained from commercial sources. The 1D ^{1}H and ^{13}C NMR and 2D ^{1}H–^{13}C HSQC, HMBC spectra in DMSO-d_6 were recorded with a Varian Unity plus-500, and standard Varian software was employed. Chemical shifts δ [ppm] were references to TMS. Notation used in the NMR assignments is given in Fig. 1.

2.1.1. 3,3′-Methanediyl-bis-indole (1)

Yield (43%). M. p. 169.8–170.0 °C.–IR (KBr): $\tilde{\nu}$=3400 (NH), 3150–3000, 3000–2800, 1620, 1600, 1460, 1430, 1220 cm^{-1}.–^{1}H NMR (500.13 MHz, DMSO-d_6): δ=4.141 (s, 2 H, 10-CH_2), 6.920 (td, 2 H, J=7.5, 1 Hz, 5-H, 5′-H), 7.032 (td, J=7.5, 1 Hz, 2 H, 6-H, 6′-H), 7.127 (d, J=2 Hz, 2 H, 2-H, 2′-H), 7.327 (d, J=7.5 Hz, 2 H, 7-H, 7′-H), 7.529 (d, J=7.5 Hz, 2 H, 4-H, 4′-H), 10.715 (s, broad, 2 H, 1-NH, 1′-NH).–^{13}C NMR (125.68 MHz, DMSO-d_6): δ=20.84 (C-10), 111.20 (C-7, C-7′), 114.13 (C-3, C-3′), 117.93 (C-5, C-5′), 118.57 (C-4, C-4′), 120.65 (C-6, C-6′), 122.65 (C-2, C-2′), 127.12 (C-8, C-8′), 136.32 (C-9, C-9′), ppm.

2.1.2. 5,5′-dinitro-3,3′-methanediyl-bis-indole (3)

Yield 33 %. M. p. 291.5-292.0 °C. decomp.–IR (KBr): $\tilde{\nu}$=3430, 3360 (N–H), 3130, 3100, 2920, 2850, 1620, 1580, 1470, 1420, 1520, 1330 (NO_2), 1220, 1130 cm^{-1}.–^{1}H NMR (500.13 MHz, DMSO-d_6): δ=4.355 (s, 2 H, CH_2), 7.532 (s, 2H, 2-H, 2′-H), 7.541 (d, J=9.0 Hz, 2 H, 7-H, 7′-H), 7.990 (dd, J=9.0, 2.0 Hz, 2 H, 6-H, 6′-H), 8.538 (d, J=2.0 Hz, 2 H, 4-H, 4′-H), 11.641 (broad s, 2 H, 1-NH, 1′-NH).–^{13}C NMR (125.68 MHz, DMSO-d_6): δ=20.24 (C-10), 111.86 (C-7, C-7′), 115.86 (C-4, C-4′), 116.41 (C-6, C-6′), 116.56 (C-3, C-3′), 126.28 (C-8, C-8′), 126.89 (C-2, C-2′), 139.60 (C-9, C-9′), 140.09 (C-5, C-5′) ppm.

2.2. X-ray diffraction measurement details

The crystal and molecular structures of **1** and **3** have been determined by X-ray diffraction. Crystals of **1** and **3** suitable for X-ray analysis were grown from methanol solution by slow evaporation. Diffraction data were collected on an Oxford Diffraction KM4CCD diffractometer [20] at 150 K, using

graphite-monochromated MoK_α radiation. A total of 787 frames were measured in six separate runs for **1** and 532 frames in four separate runs for **3**. The ω-scan was used with a step of 0.75°, two reference frames were measured after every 50 frames, they did not show any systematic changes either in peak positions or in their intensities. The unit-cells parameters were determined by least-squares treatment of setting angles of 1993 and 5761 highest intensity reflections chosen from the whole experiment for **1** and **3**, respectively. Intensity data were corrected for the Lorentz and polarization effects [21]. The structures were solved by direct methods with the SHELXS-97 program [22] and refined with full-matrix least-squares by the SHELXL-97 program [23]. The function $\Sigma w(|F_o|^2-|F_c|^2)^2$ was minimized with $w^{-1}=[\sigma^2(F_o)^{2+}(0.0431P)^2]$ for **1** and $w^{-1}=[\sigma^2(F_o)^{2+}(0.0307P)^2]$ for **3**, where $P=(F_o^2+2F_c^2)/3$. All non-hydrogen atoms were refined anisotropically, positions of hydrogen atoms were generated geometrically and their positional and isotropic displacement parameters were refined.

2.3. Electrochemical DNA biosensor assay

Preliminary studies were performed to determine the most appropriate solvent and ionic strength for dissolving the tested compounds in order to maximize solubility and obtain possibly the highest signal of DNA on the electrochemical measurements. Compounds from this group are not soluble in water solutions. Suggested organic solvents (like benzene, toluene) are potentially dangerous to DNA or can have their own affinity to nucleic bases: therefore they were not used. Only acetone, methanol and ethanol were tested as possible solvents for stock solutions. Finally, ethanol was chosen.

2.3.1. Apparatus and reagents

All electrochemical measurements were performed with a PalmSens and Palmtop analysis system with a PalmScan software package (Palm Instruments BV, Houten, The Netherlands). The planar screen-printed electrochemical cell (1.5 cm × 3.0 cm) consisted of a graphite working electrode, a graphite counter electrode and a silver pseudo-reference electrode. Screen-printed electrodes (SPEs) were printed with a Model 245 screen printer, obtained from DEK (Weimouth, UK) using different inks obtained from Acheson Italiana (Milan, Italy). The procedure and reagents to make SPEs were reported elsewhere [24]. The graphite working electrode surface area was 7 mm^2. Each electrode was disposable.

Milli-Q grade water (18 MΩ cm) was used for the preparation of all solutions. Sodium acetate, sodium chloride, potassium chloride and acetic acid were purchased from Merck and Aldrich. Double-stranded *calf thymus* DNA (dsDNA) type XV was obtained from Sigma. Concentrated stock solution of dsDNA was prepared in water and stored at −20 °C. In all experiments 50 ppm DNA solution was used in 0.25 M acetate buffer (pH 4.75) containing 10 mM KCl (AcB).

All compounds were stored in a refrigerator at 4 °C. Glass flasks and beakers were used for the preparation and intercalation step of all samples and were kept in dark because of possible hypersensitivity of the compounds to light. Appropriate amounts of the compounds were dissolved in 10 mL of pure ethanol by keeping them under stirred conditions for 30 min to obtain 4 mM concentration (stock). In the case of **3**, 1 mM stock concentration was used. Then other dilutions starting from 2 mM were prepared from the stock with AcB and ethanol to maintain the contents of 50% of ethanol till the lowest possible concentration that yielded a signal different than blank solution.

2.3.2. Electrochemical DNA biosensors

All experiments were carried out at room temperature in 5 mL beakers. Square wave voltammetry (SWV) was performed in acetate buffer [25,26] with the following parameters [27]: frequency 200 Hz, step potential 15 mV, amplitude 40 mV, potential range +0.2 – 1.45 V vs. Ag pseudo-reference electrode.

The electrode surface was pre-treated by applying a potential of +1.6 V for 120 s and +1.8 V for 60 s in AcB; this procedure was necessary to activate the electrode surface [28] and make it susceptible to the following DNA immobilization. The biosensor was developed by immobilizing dsDNA at fixed potential (+0.5 V vs. Ag pseudo-reference electrode for 300s) onto the screen-printed electrode surface, under stirred conditions. The SWV scan of immobilized dsDNA was performed for a few electrodes to evaluate the oxidation of guanine and adenine and the peak height of bases (at about +0.9 V and +1.2 V vs. Ag pseudo-reference SPE for guanine and adenine, respectively) was measured (blank). For the rest of the electrodes an interaction step was performed by sinking the electrode in a stirred solution containing the tested compound. After 2 min of incubation the sensor was washed by dipping the electrode in a clean acetate buffer solution in open-circuit condition and SWV scan was carried out. The results were reported as a peak height ratio (S%) of guanine and adenine signals (*S*% for blank = 100%),

$$S\% = (S_s/S_b) \times 100\%$$

where S_s is the guanine and adenine peak height after the interaction with a sample, and S_b is the adenine or guanine peak height after the interaction with the buffer solution alone (blank).

2.4. Pharmacology—cytotoxicity against cell lines

The in vitro cell line screening was carried out in the National Institute of Health, National Cancer Institute, Bethesda, USA, in the course of the NCI's drug discovery and development program (the details are available at web site http://dtp.nci.nih.gov).

3. Results and discussion

3.1. Electrochemical DNA biosensor assay

Square wave curves for compounds **1**, **2** and **3** in 0.25 M acetate buffer with 10 mM KCl containing 50 % of ethanol together with square wave curve of 50 ppm dsDNA in 0.25 M acetate buffer with 10 mM KCl containing 50% of ethanol are

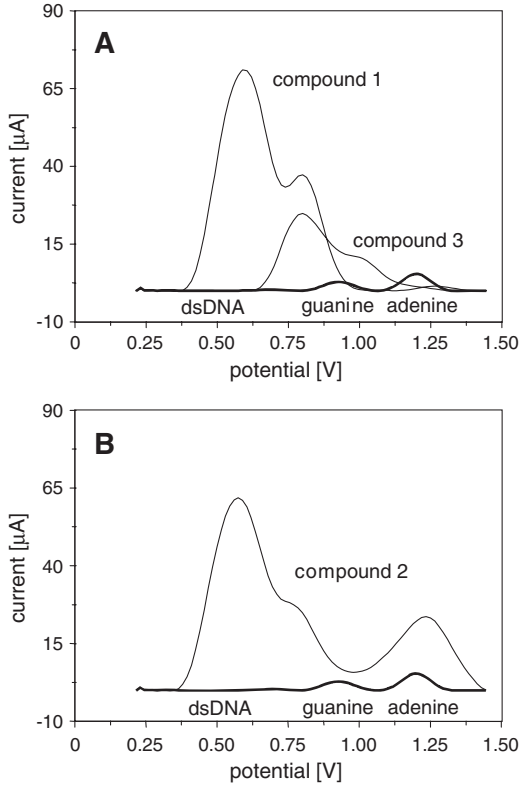

Fig. 2. Square wave curves for compounds **1**, **2** and **3** in 0.25 M acetate buffer with 10 mM KCl containing 50% of ethanol and 50 ppm dsDNA in AcB. (A) 2 mM compound **1**, 0.5 mM compound **3,** and DNA; (B) 2 mM compound **2** and DNA. Square wave parameters: frequency 200 Hz, step potential 15 mV, amplitude 40 mV, potential range: +0.2 – 1.45 V.

shown in Fig. 2A and B. DNA shows two oxidation peaks: guanine at +0.9 V and adenine at +1.2 V; *bis*-indole **1** shows two oxidation peaks: at +0.6 V and +0.8 V; *bis*-indole **2** shows three oxidation peaks: at +0.6 V, +0.8 V and +1.25 V; *bis*-indole **3** shows two oxidation peaks: at +0.8 V and +1.0 V. Separation of oxidation peaks at mM concentration allowed the accurate determination of adenine signals for DNA complexes of compounds **1** and **3**, whereas in the case of compound **2** it was impossible due to its own electro-activity.

Three peaks of **2** (Fig. 2B) coincide with DNA oxidation peaks, and this is the reason that the assay of DNA–**2** complex cannot be measured at high concentration of compound **2**— when the SWV scan is performed, two first oxidation peaks of compound **2** are very high and finding relatively low peak of guanine and separation it from plot is not possible, even if the guanine oxidation peak is not exactly at the same position as the second oxidation peak of *bis*-indole **2**. Additionally, base line for plot of compound **2** is higher than for plot of double-stranded nucleic acid, and sometimes guanine oxidation peak is just invisible.

Fig. 3 shows the trends of S% values for compounds **1**, **2** and **3** in respect of their concentration. Fig. 3A illustrates the S% changes of adenine oxidation peak at mM concentrations of compounds **1** and **3**. The correlation curve for *bis*-indole **1** was performed starting from 2 mM concentration, whereas the correlation curve for *bis*-indole **3** was performed starting from 0.5 mM, because at the concentration higher than 0.5 mM the saturated solution was obtained. It is clearly shown that attracting ability of **3** to dsDNA is much stronger than this of **1** in conditions of the assay. Compounds **1** and **3** at the concentration of 0.5 mM reduce the adenine signal to 64% and 23%, respectively. *Bis*-indole **1**, even if is less active, reduces the adenine signal to 36% at the highest concentration tested (2 mM). The results show clearly that the substituent replacement at C5 and C5′ positions in *bis*-indoles changes significantly the DNA binding properties of these compounds at mM concentration in solutions.

As mentioned above, the oxidation peaks of compounds **1**, **2** and **3** at mM concentration level coincides with the peak of DNA guanine oxidation (it is not possible to separate peaks of dsDNA and tested substances, when SWV scan is performed with DNA and interacted compound). That is why we

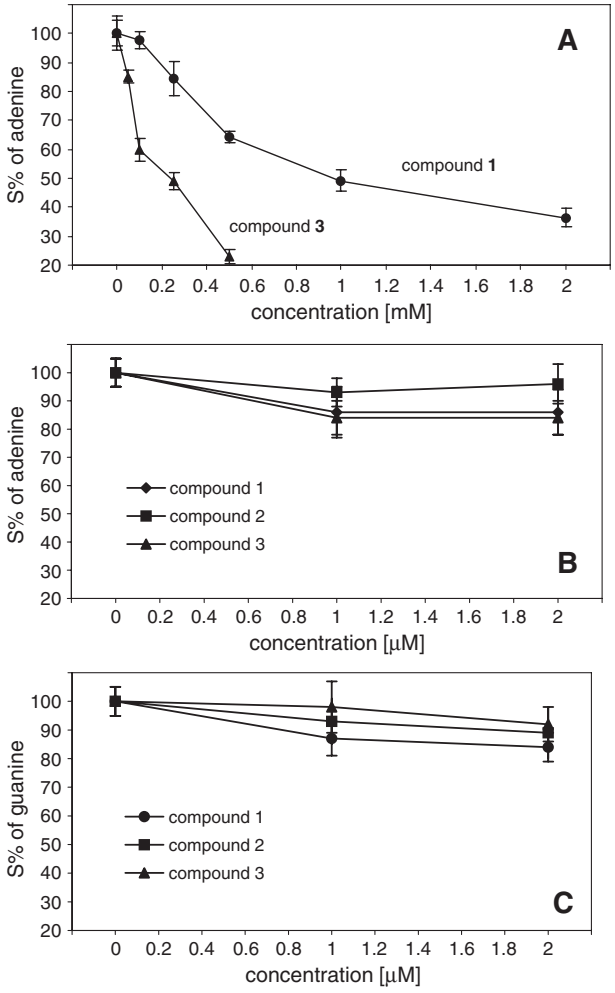

Fig. 3. Comparison of adenine signal ratio obtained from the tested compounds in 0.25 M acetate buffer with 10 mM KCl containing 50% of ethanol, compounds **1** and **3** (A) and low concentrations of all compounds (B); signals of guanine of all compounds for low concentrations (C). Electrode conditioning: +1.6 V for 120 s and +1.8 V for 60 s vs. Ag pseudo-reference screen-printed electrode. DNA immobilization: 300 s at 0.5 V vs. Ag pseudo-reference SPE. Interaction time: 2 min in open-circuit conditions. Square wave parameters: frequency 200 Hz, step potential 15 mV, amplitude 40 mV, potential range: +0.2 – 1.45 V.

Table 1
The 50% growth inhibition values (GI_{50} in molar units) of 5,5′-dimethoxy-3,3′-methanediyl-*bis*-indole together with mean graph midpoints (MS-MID) for all human cancer cell lines tested

Cell lines	Lung cancer HOP-92	Renal cancer A 498	Breast Cancer MDA-MB-231/ATCC	MG-MID (log_{10})		
				GI_{50} ihibitory effect	TGI cytostatic effect	LC_{50} cytotoxic effect
$log_{10}G_{I50}$	−7.48	−5.48	−5.33	−4.77	−4.35	−4.10

investigated both, adenine (Fig. 3B) and guanine (Fig. 3C) oxidation signal changes of all the compounds tested at much lower concentration, namely at micro molar (μM), where the height of oxidation peaks of substances is lower than detection limit, and does not interfere in DNA analysis. *Bis*-indole **1** and **3** at 2 μM concentration decrease the adenine oxidation signal in the same extend (down to 80%). The differences between these compounds and blank are statistically significant (Student's group *t*-test for independent samples; $n_{blank}=5$, $n_{compound\ 1}=5$, $n_{compound\ 3}=4$; $t_{exp\ (blank\text{-}compound\ 1)}=2.83$, $t_{exp\ (blank\text{-}compound\ 3)}=3.99$, $t_{max(f=8)}=2.31$, $t_{max(f=7)}=2.36$; the level of confidence $(1-\alpha)=0.95$), while the effect of *bis*-indole **2** in comparison with blank solution is not statistically significant (Student's group *t*-test for independent samples; $n_{blank}=5$, $n_{compound\ 2}=4$, $t_{exp\ (blank\text{-}compound\ 2)}=0.75$, $t_{max(f=7)}=2.36$; $(1-\alpha)=0.95$). It means that compound **2** shows less affinity to dsDNA than *bis*-indoles **1** and **3** at adenine-thymine rich region. At the same time the guanine oxidation signal is changed (down to 85%) in presence of all tested compounds **1**, **2**, **3** in the following order: **1**>**2**>**3**. Despite the fact that statistical analysis have elucidated that these changes among *bis*-indoles at μM concentrations are not statistically significant, importance of differences was observed for 2 μM compound **1** in comparison with blank solution (t-Student group test for independent samples; $n_{blank}=5$, $n_{compound\ 1}=5$, $t_{exp\ (blank\text{-}compound\ 1)}=4.41$, $t_{max(f=8)}=2.31$; $(1-\alpha)=0.95$). The magnitude of nucleic bases oxidation changes is closely related to the affinity of the interaction of tested compounds with double-helix DNA: the greater decrease, the stronger interaction with nucleic acid.

Table 2
Crystal data, data collection and structure refinement for compounds **1** and **3**

Compound	**1**	**3**
Empirical formula	$C_{17}H_{14}N_2$	$C_{17}H_{12}N_4O_4$
Formula weight	246.30	336.31
T (K)	150(2)	150(2)
Wavelength (Å)	0.71073	0.71073
Crystal system, space group	monoclinic, *C* 2/c	monoclinic, *C* 2/c
Unit cell dimensions		
a (Å)	27.142(4)	31.742(2)
b (Å)	5.720(1)	13.289(1)
c (Å)	8.302(1)	15.993(1)
β (°)	106.50(1)	117.29(1)
Volume ($Å^3$)	1235.8(3)	5995.3(7)
Z, D_x (Mg/m^3)	4, 1.324	16, 1.490
μ (mm^{-1})	0.079	0.110
F (000)	520	2784
θ range for data collection (°)	3.65–30.06	5.24–29.33
hkl range	$-33\le h\le 37$	$-43\le h\le 41$
	$-8\le k\le 7$	$-17\le k\le 13$
	$-11\le l\le 7$	$-21\le l\le 22$
Reflections		
collected	5880	19 797
unique (R_{int})	1651(0.037)	7532(0.036)
observed ($I>2\sigma(I)$)	1040	4051
Data/restraints/parameters	1651/0/115	7532/0/547
Goodness-of-fit on F^2	0.911	0.843
$R(F)(I>2\sigma(I))$	0.0396	0.0389
$wR(F^2)$ (all data)	0.0880	0.0784
Max/min. $\Delta\rho$ ($e/Å^3$)	0.184/−0.248	0.171/−0.245

3.2. Cytotoxicity against cancer cell lines

Compound **2** was passed on for evaluation in the full panel of 60 different cell lines, representing human leukemia, non-small cell lung cancer, colon cancer, CNS (central nervous system) cancer, melanoma, ovarian cancer, renal cancer, prostate cancer and breast cancer cell lines. The results from representative cell lines are listed in Table 1, along with mean graph midpoint (MG-MID) values for all 60 lines.

The 5,5′-dimethoxy-3,3′-methanediyl-*bis*-indole (**2**) was found to reduce considerably the growth of cancer cell lines HOP-92 (lung), A498 (renal) and MDA-MB-231/1TCC (breast) in a dose dependent manner. Although compound **2** proved to afford a high mean graph value of cytotoxicity, intensity and location of its oxidation peaks did not allow its electrochemical screening (discussion in Section 3.1).

3.3. NMR spectra

So far, no complete assignments of ^1H and ^{13}C NMR resonances for the reported compounds **1** and **3** have been published. The resolution of signals pattern was not an easy

Table 3
Selected bond lengths [Å] and angles [°] and selected torsional angles [°] of **1** and **3**

	1	**3**	
		Molecule A	Molecule B
N1-C9	1.373(1)	1.365(2)	1.357(2)
N1′-C9′	1.373(1)	1.360(2)	1.364(2)
N1-C2	1.377(2)	1.378(2)	1.380(2)
N1′-C2′	1.377(2)	1.385(2)	1.383(2)
C2-C3	1.368(2)	1.354(2)	1.360(2)
C2′-C3′	1.368(2)	1.355(2)	1.364(2)
C8-C9	1.417(2)	1.420(2)	1.424(2)
C8′-C9′	1.417(2)	1.419(2)	1.420(2)
C9-N1-C2	109.0(1)	109.0(1)	109.4(1)
C9′-N1′-C2′	109.0(1)	109.1(1)	109.1(1)
C3-C10-C3′	114.8(1)	115.8(1)	113.7(1)
C8-C3-C10-C3′	−145.9(1)	−72.3(2)	168.5(1)
C8′-C3′-C10-C3	−145.9(1)	−172.6(1)	−109.6(2)
N1-C2-C3-C10	177.3(1)	177.8(1)	179.2(1)
N1′-C2′-C3′-C10	177.3(1)	−178.4(1)	−177.4(1)

Table 4
Hydrogen-bonding geometry [Å and °] of **1** and **3**

Compound **1**				
D–H···A	d(D–H)	d(H···A)	d(D···A)	<(DHA)
N1–H1···Cg^{I}	0.91(1)	2.47(1)	3.178(1)	135(1)

Cg represents the centroid of six-membered ring of the indole; symmetry code: (i) $x, -y, 0.5+z$.

Compound **3**				
*N1–H1···O12′ ^{i}	0.86(1)	2.24(1)	3.012(2)	149(1)
*N1–H1···O12A^{i}	0.86(1)	2.41(1)	2.975(2)	123(1)
*N1A–H1A···O12^{ii}	0.87(2)	2.15(2)	2.981(2)	160(1)
*N1A–H1A···O13^{ii}	0.87(2)	2.45(2)	3.187(2)	143(1)
N1′–H1′···O12B^{iii}	0.87(2)	2.13(2)	2.935(2)	153(1)
N1′–H1′···O13B^{iii}	0.87(2)	2.59(2)	3.390(2)	153(1)
*N1′A–H1′A···O13A^{i}	0.91(2)	2.18(2)	3.008(2)	150(1)
N1′A–H1′A···O13′ ^{iv}	0.91(2)	2.55(2)	3.196(2)	129(1)
C7–H7···O12′ ^{i}	0.95(1)	2.75(1)	3.442(2)	130(1)
C7′A–H7′A···O13A^{i}	0.98(1)	2.83(1)	3.523(2)	128(1)
C7–H7···O12B^{v}	0.95(1)	2.78(1)	3.443(2)	127(1)
C6′–H6′···O13^{vi}	0.95(1)	2.44(1)	3.292(2)	149(1)
C10A–H10B···O13A^{iv}	0.99(1)	2.75(2)	3.712(2)	164(1)
C2′A–H2′A···O12A^{iv}	0.99(1)	2.59(1)	3.346(2)	133(1)
C6′A–H6′A···O12^{vii}	0.99(2)	2.70(1)	3.353(2)	124(1)
C7A–H7A···O13^{ii}	0.92(1)	2.78(1)	3.471(2)	132(1)

Symmetry codes: (i) $x, -1+y, z$; (ii) $0.5+x, 0.5+y, z$; (iii) $-x$, y, $-0.5-z$; (iv) $0.5-x, -0.5+y, 0.5-z$; (v) $x, -1-y, 0.5+z$; (vi) $-x, -y, -z$; (vii) $-x, -1-y, -z$.

task, and the 2D hetero- and homonuclear NMR experiments were used to obtain complete assignment. We have observed a standard pattern of signals, i.e. the number of peaks was equal to the number of chemically distinct sites in the molecules. This indicates that no steric hindrance occurs in solution, when indole rings rotate around the methylene linker. The assignments of resonances are given in Section 2.1.

3.4. X-ray structure

The crystallographic data, together with data collection and structure refinement details are listed in Table 2. Selected bond lengths, bond angles and torsion angles are listed in Table 3, and hydrogen bonding parameters in Table 4.

Additional crystallographic data have been deposited with the Cambridge Crystallographic Data Centre as supplementary publications CCDC 280793 and 280794. The displacement ellipsoid representation of the molecules, together with the atomic numbering scheme, is shown in Fig. 4 (the drawings were performed with a Stereochemical Workstation [29]). Figs. 5–7 show various packing arrangements of **1** and **3**.

The compounds crystallize in the monoclinic space group C 2/c with a half of the ordered molecule in the asymmetric unit for **1** (the molecule occupies a special position: the C10 atom is located at two-fold axis) and two molecules for **3**. The structures consist of two indole systems connected through a common C atom (C10). The molecular geometries of both compounds are similar and quite typical. Bond lengths observed in the molecules vary insignificantly (Table 3) and they are in good agreement with the corresponding distances in the related compounds [14,30].

The indole fragments are essentially planar to within 0.010(1) Å for **1** and 0.024(1) Å for **3** with the dihedral angle between their mean planes of 61.21(2)° for **1**, 69.55(3)° and 65.81(3)° for the two independent molecules of **3**. A similar dihedral angle was also observed for **2** [14]. Nevertheless the

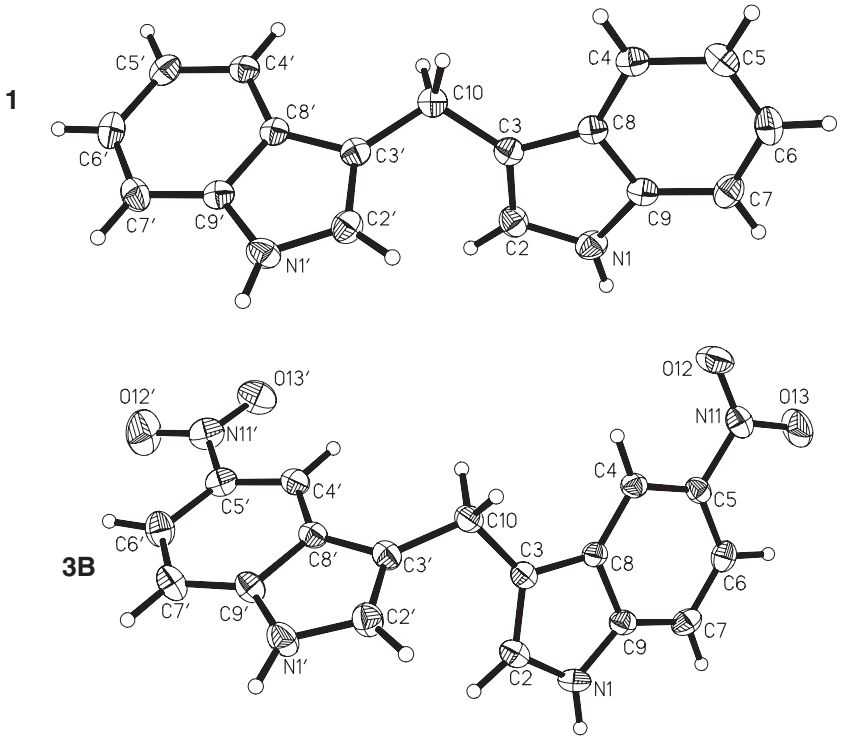

Fig. 4. Molecular structure of **1** and **3B** with 50% probability displacement ellipsoids and atom-numbering scheme.

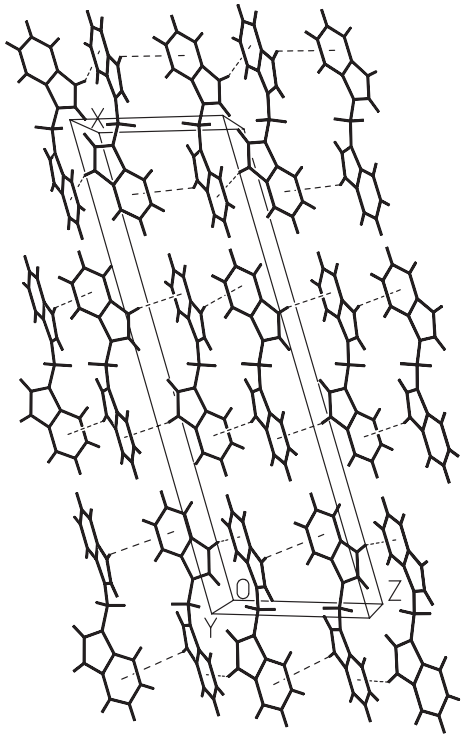

Fig. 5. Projection of the crystal structure of **1** along the *b* axis with N–H···π intermolecular hydrogen-bonding interactions.

molecular structures of **1**, **2** and **3** differ in the arrangement of these fragments. The appropriate torsion angles for **1** and **3** are given in Table 2, for **2** in [14]. The other non-H atoms in **1** and **3** are found to be only marginally out of the planes of the two-ring frameworks.

In the crystals of **1**, **2** and **3**, the packing of the molecules is stabilized by different weak intermolecular hydrogen-bondings interactions. The geometric parameters of these bonds for **1** and **3** are given in Table 3. The crystal structure of **1** is built of infinite chains of molecules connected via N–H···π intermolecular interactions along the *c* axis (Fig. 5).

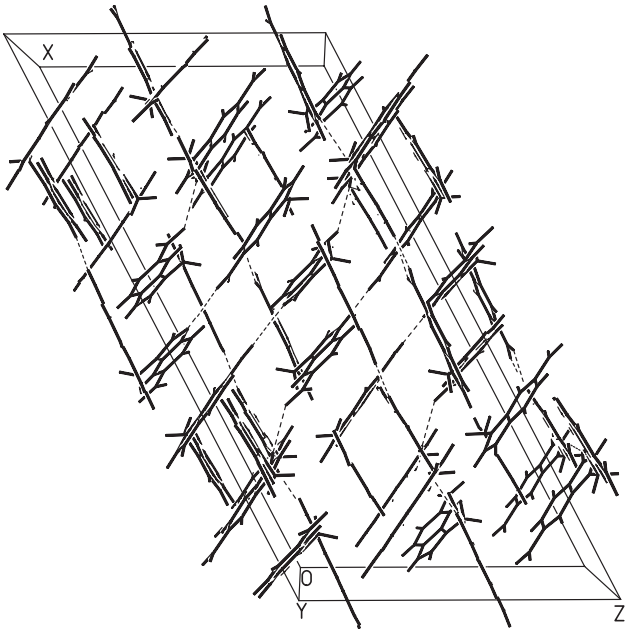

Fig. 7. Projection of the crystal structure of **3** along the *b* axis with N–H···O intermolecular hydrogen-bonding interactions.

Similar N–H···π interactions were observed for **2** [14], other indole derivatives [31,32] and for globular proteins [33]. It has been suggested that such interactions may provide stability, and may contribute to the folding process or have a functional role in proteins.

In the crystal of **3**, there is a three-dimensional network of N–H···O and C–H···O intermolecular interactions. The molecules are linked by some of the N–H···O hydrogen bonds (with *—see Table 3) into layers parallel to (001) (Fig. 6). Cohesion between these layers results from the remaining N–H···O contacts. The oxygen atoms are also involved in numerous intermolecular C–H···O interaction [34], which result from the crystal packing of the molecules. The packing arrangement is shown in Fig. 7.

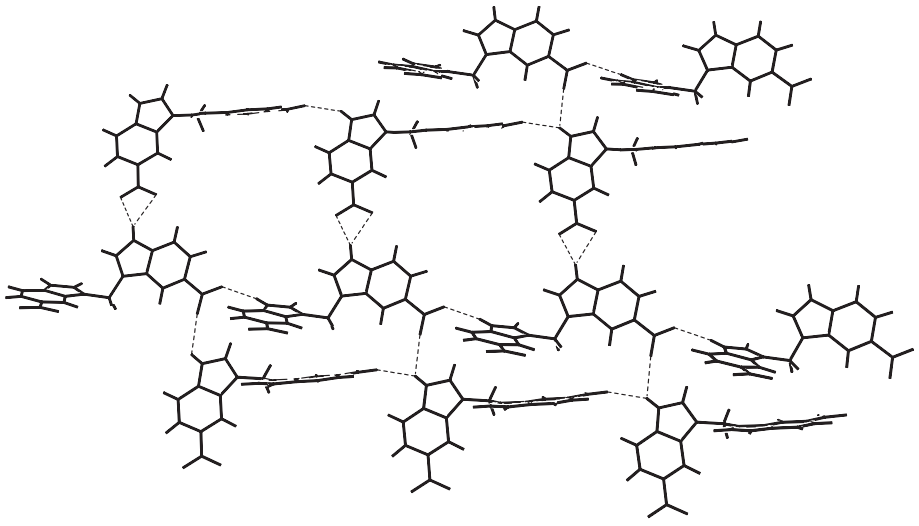

Fig. 6. A view showing the interconnections within one layer for **3**.

In the case of derivatives **1** and **2** we have observed the interaction between the NH groups and π-electron system of indole rings which is not present in derivative **3**. This is reasonable because the NH···π interaction may increase on replacement of the substituent H by the electron-donating OCH_3 groups (in **2**). The inverse should be true for compound **3** with the electron-accepting NO_2 substituents. Instead, in the crystals of compound **3**, the oxygen atoms of nitro groups are involved in many types of hydrogen bonds (Table 4). The NH···π interaction should be characteristic of a relatively large contribution from charge transfer from π to σ^* orbital as compared with regular H-bonding. Both kinds of interaction are important to understand of the behavior of a dynamically interacting molecular system. We can thus put forward a hypothesis that the tested *bis*-indoles **1** and **2** are therefore capable of forming the NH···π interacted complexes of nucleic acids, whereas *bis*-indole **3** is able to form a favorable H-bond interaction as a guest molecule incorporated in analogous complexes. From this point of view, the electrochemical DNA bioassay results (see Section 3.1) could be interpreted in terms of attractive interactions of both types, however the importance of H-bonds should be considered as particularly effective.

4. Conclusions

The presented electrochemical DNA biosensor indicates the grade of binding of a molecule to deoxyribonucleic acid. The tests provided with this kind of sensors can give fast and reliable information about affinity of chemical compounds and their behavior in the presence of DNA [35]. This can be helpful while working on new antitumor drugs before performing very expensive tests and analyses. On the basis of electrochemical measurements we have hypothesized that the analyzed *bis*-indoles have an effect on human tumor cells due to DNA binding at AT-rich region in a concentration/substituent dependent manner. However, we cannot define the binding affinity of those compounds to GC-rich region at high concentration. The results at low micro molar concentration also show the binding properties of investigated *bis*-indoles at AT-rich regions, and statistically less meaningful at GC-rich regions.

The results of X-ray analysis indicate insignificantly different molecular geometries of the investigated compounds and significantly different networks of intermolecular interactions in crystals. The tested *bis*-indoles could be involved in the NH···π and H-bond intermolecular interactions with the nucleic acid, which could be responsible for their cytotoxity. According to ^1H and ^{13}C NMR data no hindered rotation phenomena are observed in solution.

References

[1] M. Minunni, S. Tombelli, E. Mariotti, M. Mascini, M. Mascini, Biosensors as new analytical tool for detection of Genetically Modified Organisms (GMOs), Fresenius, J. Anal. Chem. 369 (2001) 589–593.
[2] S. Rauf, J.J. Gooding, K. Akhtar, M.A. Ghauri, M. Rahman, M.A. Anwar, A.M. Khalid, Electrochemical approach of anticancer drugs–DNA interaction, J. Pharm. Biomed. Anal. 37 (2005) 205–217.
[3] B. Meric, K. Kerman, D. Ozkan, P. Kara, S. Erensoy, U.S. Akarca, M. Mascini, M. Ozsoz, Electrochemical DNA biosensor for the detection of TT and Hepatitis B virus from PCR amplified real samples by using methylene blue, Talanta 56 (2002) 837–846.
[4] L.W. Wattenberg, W.D. Loub, Inhibition of polycyclic aromatic hydrocarbon-induced neoplasia by naturally occurring indoles, Cancer Res. 38 (1978) 1410–1413.
[5] G.S. Bailey, J.D. Hendricks, D.W. Shelton, J.E. Nixon, N.E. Pawlowski, Enhancement of carcinogenesis by the natural anticarcinogen indole-3-carbinol, J. Natl. Cancer Inst. 78 (1987) 931–934.
[6] D.E. Williams, R.H. Dashwood, J.D. Henricks, G.S. Bailey, in: S.L. Taylor, R.A. Scanlan (Eds.), Food Toxicology A Perspective on the Relative Risks, Marcel Dekker, New York, 1990, pp. 101–150.
[7] C.J. Grubbs, V.E. Steele, T. Casebolt, M.M. Juliana, I. Eto, L.M. Whitaker, K.H. Dragnev, G.J. Kellof, R.L. Lubet, Chemoprevention of chemically-induced mammary carcinogenesis by indole-3-carbinol, Anticancer Res. 15 (1995) 709–716.
[8] C.M. Cover, S.J. Hsieh, S.H. Tran, G. Hallden, G.S. Kim, L.F. Bjendales, G.L. Firestone, Indole-3-carbinol inhibits the expression of cyclin-dependent kinase-6 and induces a G1 cell cycle arrest of human breast cancer cells independent of estrogen receptor signaling, J. Biol. Chem. 273 (1998) 3838–3847.
[9] C. Hong, G.L. Firestone, L.F. Bjeldanes, Bcl-2 family-mediated apoptotic effects of 3,3′-diindolylmethane (DIM) in human breast cancer cells, Biochem. Pharmacol. 63 (2002) 1085–1097.
[10] D.J. Kim, B.S. Han, B. Ahn, R. Hasegawa, T. Shirai, N. Ito, H. Tsuda, Enhancement by indole-3-carbinol of liver and thyroid gland neoplastic development in a rat medium-term multiorgan carcinogenesis model, Carcinogenesis 18 (1997) 377–381.
[11] C. Hong, H.-A. Kim, G.L. Firestone, L.F. Bjeldanes, 3,3′-diindolylmethane (DIM) induces a G1 cell cycle arrest in human breast cancer cells that is accompanied by Sp1-mediated activation of $p21^{WAF1/CIP1}$ expression, Carcinogenesis 23 (2002) 1297–1305.
[12] G.L. Firestone, L.F. Bjeldanes, Indole-3-carbinol and 3,3′-diindolylmethane antiproliferative signaling pathways control cell-cycle gene transcription in human breast cancer cells by regulating promoter-Sp1 transcription factor interaction, J. Nutr. 133 (2003) 2448S–2455S.
[13] T.A. Larsen, D.S. Goodsell, D. Cassio, K. Grześkowiak, R.E. Dickerson, The structure of 4′-6-diamidine-2-phenylindole bound to synthetic DNA, J. Biomol. Struct. Dyn. 7 (1989) 477–491.
[14] D. Maciejewska, M. Niemyjska, I. Wolska, M. Włostowski, M. Rasztawicka, Synthesis, spectroscopic studies and crystal structure of 5,5′-dimethoxy-3,3′-methanediyl-*bis*-indole as the inhibitor of cell proliferation of human tumors, Z. Naturforsch. 59b (2004) 1137–1142.
[15] J. Wang, G. Rivas, X. Cai, E. Palecek, P. Nielsen, H. Shirashi, N. Dontha, D. Luo, C. Parrado, M. Chicarro, P.A.M. Farias, F.S. Valera, D.H. Grant, M. Ozsoz, M.N. Flair, DNA electrochemical biosensors for environmental monitoring, Anal. Chim. Acta 347 (1997) 1–8.
[16] E. Palecek, M. Fojta, DNA hybridization and damage, Anal. Chem. 73 (2001) 74A–83A.
[17] J. Wang, M. Ozsoz, X. Cai, G. Rivas, H. Shirashi, D.H. Grant, M. Chicharro, J. Fernandes, E. Palecek, Interaction of antitumor drug daunomycin with DNA in solution and at the surface, Bioelectrochem. Bioenerg. 45 (1998) 33–40.
[18] J. Thesing, Beiträge zur Chemie des Indols. III Mitteil: Über die Einwirkung von Alkali auf quartäre Saze des Gramins, Chem. Ber. 31 (1954) 692–699.
[19] S. Földeak, J. Czombos, B. Matkowics, Synthesis of new diindolylmethane derivatives effecting C.N.S., Acta Phys. Chem. 11 (1965) 115–125.
[20] Oxford Diffraction Poland, CrysAlisCCD, CCD Data Collection GUI, version 1.171 (2003).
[21] Oxford Diffraction Poland, CrysAlisRED, CCD data reduction GUI, version 1.171 (2003).
[22] G.M. Sheldrick, Phase annealing in SHELX-90: direct methods for larger structures, Acta Crystallogr., A 46 (1990) 467–473.
[23] G.M. Sheldrick, SHELXL97, Program for the Refinement of Crystal Structures, University of Göttingen, Germany, 1997.

[24] A. Cagnini, I. Palchetti, I. Lionti, M. Mascini, A.P.F. Turner, Disposable ruthenized screen printed biosensors, Sens. Actuators, B, Chem. 24 (1995) 85–89.
[25] G. Chiti, G. Marazza, M. Mascini, Electrochemical DNA biosensor for environmental monitoring, Anal. Chim. Acta 427 (2001) 155–164.
[26] M. Mascini, I. Palchetti, G. Marazza, DNA electrochemical biosensors, Fresenius' J. Anal. Chem. 369 (2001) 15–22.
[27] F. Lucarelli, A. Kicela, I. Palchetti, G. Marazza, M. Mascini, Electrochemical DNA biosensor for analysis of wastewater samples, Bioelectrochemistry 58 (2002) 113–118.
[28] M.E. Rice, Z. Galus, R.N. Adams, Graphite paste electrodes. Effects of paste composition and surface states on electron-transfer rates, J. Electroanal. Chem. 143 (1983) 89–102.
[29] Stereochemical Workstation Operation Manual, Release 3.4. Siemens Analytical X-ray Instruments Inc., Madison, Wisconsin, USA, 1989.
[30] F.H. Allen, Acta Crystallogr., B 58 (2002) 380–388 (CSD, Version 5.25 of November 2003 and three updates).
[31] R. Krishna, D. Velmurugan, G. Babu, P.T. Perumal, N–H···π(indole) intermolecular interactions in 3,3′-benzylidenediindole, Acta Crystallogr., C Cryst. Struct. Commun. C55 (1999) 75–78.
[32] R. Krishna, D. Velmurugan, S. Shanmuga Sundara, *Bis*(indol-3-yl)(4-methylphenyl)methane, Acta Crystallogr., C Cryst. Struct. Commun. 55 (1999) (IUC9900084).
[33] M. Crisma, F. Formaggio, G. Valle, C. Toniolo, M. Saviano, R. Lacovino, L. Zaccaro, E. Benedetti, Experimental evidence at atomic resolution for intramolecular N–H···π(phenyl) interactions in a family of amino acid derivatives, Biopolymers 42 (1997) 1–6.
[34] G.R. Desiraju, The C–H···O hydrogen bond: structural implications and supramolecular design, Acc. Chem. Res. 29 (1996) 441–449.
[35] M. Ravera, S. Baracco, C. Cassino, D. Colangelo, G. Bagni, G. Sava, D. Osella, Electrochemical measurements confirm the preferential bonding of the antimetastatic complex [ImH][RuCl4(DMSO)(Im)] (NAMI-A) with proteins and the weak interaction with nucleobases, J. Inorg. Biochem. 98 (2004) 984–990.